

# N-body Simulations of Galactic Components

A570: Final Project

Greg Lukens

April 26, 2021

## Abstract

In this paper, the dynamical effects of an N-body simulation with a disk, a stellar halo, and a bulge, a disk and a stellar halo, and an isolated disk are analyzed. The simulations were run using a massively parallel hybrid tree-smoothed-particle-hydrodynamics code (*TreeSPH*) GADGET-2. Understanding the simulated evolution of galactic density profiles, velocity dispersion profiles, and rotation curves is of great importance to the field of galactic dynamics. In all three simulations, the emergence of a large-scale structure is observed in the disk and in the bulge (when it is included). While it may be due to issues in the initialization of the disk and bulge velocities, it is possible that this phenomenon represents a spherically-symmetric realization of an anti-axisymmetric mode, such as a bar or spiral arms.

# 1 Introduction

The goal of this project was to analyze the dynamical evolution and stability of various N-body simulations of a spiral galaxy. Specifically, I will discuss the change over time of density profiles, positions of stars, circular velocities, and velocity dispersion profiles, as well as a few other important quantities.

These simulations were conducted over three setups, listed in order of computational difficulty from slowest to fastest: all three stellar components (disk, halo, and bulge), disk and halo, and an isolated disk. Simulations such as these are crucial to understanding the dynamical processes involved in galaxy formation, star formation, and cosmology.

The use of the word “stellar” is of paramount importance, as will be seen in the rotation curves in the results section; there is no dark matter in these simulations. The halos, while distributed according to dark matter halo profiles, contain luminous matter only.

The simulations presented in this paper were run using *GADGET-2*, a massively parallel cosmological *TreeSPH* code (see [Springel 2005 \[6\]](#)). The simulations were run on Indiana University’s large memory computer cluster, Carbonate, which was accessed virtually.

One of the main findings of these simulations is that due to the immense scale of the initial conditions in the first two runs, the outer disk hardly changed dynamically. In other words, the simulations involving a halo or bulge (or both) took too long to run to simulate the long-term development of the entire disk. However, in the case of the isolated disk, the computational run-time was much shorter, so we were able to see some development of the outer disk.

As will be discussed in the next section in more detail, the most difficult aspect of running N-body simulations is setting up the initial conditions in some form of equilibrium or pseudo-equilibrium. I used one of the more predominant publications about initial conditions in simulations to help initialize our galaxy ([Hernquist 1993 \[3\]](#))

The long-term stability of disks is of partic-

ular interest (hence the longer run-time for the isolated disk). It has been known from past N-body simulations that disks initialized in complicated gravitational potentials tend towards expanding radially outward if the velocities of disk stars are even slightly off from equilibrium ([McMillan & Dehnen 2007 \[4\]](#)). If the disk was expanding in a short dynamical time, it was an indicator that the initial conditions were flawed in some manner when running the simulations.

From a computational standpoint, the density and velocity dispersion profiles of each stellar component were measured using cylindrical shells for the disk and spherical shells for the halo and bulge. All of these structures were formed via fixed bins of stars.

Specifically, 1000 stars were contained in each cylindrical shell of the disk when measuring the radial density component, and 100 stars were contained in each shell when measuring the vertical component. For the disk and bulge, 1000 stars were contained in each shell when measuring density. For all velocity dispersion plots, only 100 stars were used for each type of shell.

In order to measure dispersion, the standard deviation of the corresponding velocity component was taken over all of the stars in a given shell. In order to measure density, the number of stars in the shell (fixed) was divided by the volume/area of the shell.

The appendix will contain a link to all of the codes used to initialize the galaxies and analyze the outputs of the simulations. All codes were created using Python.

# 2 Setup

## 2.1 The Disk

As mentioned before, the Hernquist paper was of particular importance to setting up the initial conditions of the simulated galaxy. All of the components of the galaxy were initialized starting from density profiles, as is customary. The disk was setup assuming locally isothermal sheets in the ver-

tical direction ( $z$ ) and an exponential profile in the radial direction.

$$\rho_d(R, z) = \Sigma(R)\zeta(z) \quad (1)$$

$$\rho_d(R, z) = \frac{M_d}{4\pi R_d^2 z_d} e^{-R/R_d} \operatorname{sech}^2\left(\frac{z}{z_d}\right) \quad (2)$$

Here the disk density profile is separated into a surface density (given by the exponential profile) and a vertical density (given by the squared hyperbolic secant). The values  $R_d$  and  $z_d$  are the scale radius and scale height of the disk, respectively.  $M_d$  is the total mass of the disk. The values used for these parameters are listed in Table 1.

The closed form of the gravitational potential for a disk with this density profile is extremely complicated, so in order to simplify things, the spherical approximation for an exponential disk profile was used.

$$\Phi_d(r) = -GM_d \left( \frac{1 - e^{-r/R_d}}{r} \right) \quad (3)$$

where  $r = \sqrt{R^2 + z^2}$ . The positions of the disk stars were initialized from the radial mass distribution and vertical mass distribution in a similar manner to the density in equation 1.

The velocities of the disk were mainly initialized around the circular velocity, with some noise added from specific velocity dispersion equations. Recall the definition of circular velocity.

$$v_c(r) = \sqrt{r \frac{d\Phi_d}{dr}} \quad (4)$$

The velocity dispersion equations for each coordinate were given by Hernquist. The mean velocity in the  $z$  direction and radial direction were both assumed to be 0 for the disk. The dispersions in those directions were given as follows:

$$\overline{v_R^2} = \alpha e^{-R/R_d} \quad (5)$$

$$\overline{v_z^2} = \pi G z_d \Sigma(0) e^{-R/R_d} \quad (6)$$

Here  $\alpha$  is a proportionality constant and  $\Sigma(0)$  is the central surface density. As will be discussed in a later section, the value of  $\Sigma(0)$  was severely down-scaled in the creation of the disk, so the  $z$  velocities ended up scaled down by a large factor.

For the azimuthal velocity dispersion, the mean velocity was *not* zero, so the velocity dispersion is written in terms of a  $\sigma$  rather than the squared-mean. Hernquist utilized the epicycle frequency and angular frequency in his construction of the azimuthal dispersion.

$$\kappa^2 = \frac{3}{R} \frac{\partial \Phi}{\partial R} + \frac{\partial^2 \Phi}{\partial R^2} \quad (7)$$

$$\Omega = \frac{v_c}{R} \quad (8)$$

$$\sigma_\phi^2 = \overline{v_R^2} \frac{\kappa^2}{4\Omega^2} \quad (9)$$

Here,  $\kappa$  represents the epicycle frequency.  $\Phi$  in this case is the total potential of the system. In equation 7 it is assumed that the partial derivative of the actual disk potential with respect to the radial coordinate is approximately equal to the total derivative of the spherical approximation of the potential with respect to radius.

$\Omega$  represents the angular frequency, and  $\sigma_\phi^2$  represents the azimuthal velocity dispersion. Now that these have been generated, we turn our attention to the mean azimuthal velocity, which is given as the following:

$$\overline{v_\phi^2} = \overline{v_R^2} \left( 1 - \frac{\kappa^2}{4\Omega^2} - 2 \frac{R_d}{z_d} \right) + v_c^2 \quad (10)$$

Therefore, the azimuthal velocities of each disk star were initialized from a Gaussian distribution centered around the mean azimuthal velocity and with a standard deviation given by the square root of the dispersion. The same procedure was used for the other two components of velocity. Once all of the cylindrical velocity coordinates were found, the Cartesian velocities were assigned assuming the standard coordinate transformations.

## 2.2 The Halo

The way the halo was initialized in the simulations differs from Hernquist's setup. He went with a modified exponential profile with a cutoff radius, whereas I took advantage of the Navarro-Frenk-White (NFW) model, which is given as the following ([Navarro et al. 1996 \[5\]](#)):

$$\rho_h(r) = \frac{M_h}{4\pi} \frac{1}{r(r+a_h)^2} \quad (11)$$

In this equation,  $a_h$  represents the scale radius of the halo, and  $M_h$  represents the mass of the halo is given by  $M_h$ . It should actually be noted that the NFW mass profile is divergent, so it would be more proper to denote  $M_h$  as the mass out to some finite radius.

The potential for the NFW profile is given as the following:

$$\Phi_h(r) = -\frac{GM_h}{r} \ln \left( 1 + \frac{r}{a_h} \right) \quad (12)$$

The velocities of the halo stars were determined from the radial velocity dispersion, assuming isotropy. The radial dispersion was given by the following equation:

$$\overline{v_r^2} = \frac{1}{\rho_h(r)} \int_r^\infty \rho_h(r) \frac{d\Phi}{dr} dr \quad (13)$$

where, as was the case for the disk epicycle frequency,  $\Phi$  represents the total potential of the system, not just the halo potential. Using this equation, we can find the speeds of the halo stars, which are chosen randomly from a distribution which has a second moment equal to  $\overline{v_r^2}$ .

The function chosen in the Hernquist paper and again in these simulations was the normalized Maxwell probability distribution. Specifically,

$$F(v, r) = \sqrt{\frac{2}{\pi}} \frac{v^2}{\overline{v_r^2}} e^{-v^2/2\overline{v_r^2}} \quad (14)$$

Halo star speeds were limited to be less than  $0.95v_{esc}$ , where the escape velocity is given by

$$v_{esc} = \sqrt{2|\Phi|} \quad (15)$$

This cutoff, as explained by Hernquist, is empirically better than restricting to just below the escape velocity.

To create the effect of isotropy, the speeds were then converted to a randomized set of spherical coordinates (different from the position coordinates).

## 2.3 The Bulge

The way the bulge was initialized differs slightly from Hernquist's method. He opts for a triaxial (in other words, convoluted) setup, whereas in the case of my simulations, the Hernquist density profile was utilized ([Hernquist 1990 \[2\]](#)).

$$\rho_b(r) = \frac{M_b}{2\pi} \frac{a_b}{r(r+a_b)^3} \quad (16)$$

In the above equation,  $a_b$  represents the scale radius of the bulge. The potential of the bulge, therefore, is given by the following equation:

$$\Phi_b(r) = -\frac{GM_b}{(r+a_b)} \quad (17)$$

In order to simulate a similar isotropic distribution to that of the halo, the bulge velocities and radial dispersion were setup in the same way.

Therefore, the radial dispersion of the bulge was given by equation 13, where instead of  $\rho_h(r)$ ,  $\rho_b(r)$  was used. The speeds were then drawn from the same distribution function (see equation 14), with the upper bound being the escape velocity (instead of 95% of it) and again, a similar procedure of assigning the velocity coordinates was followed assuming isotropy.

As will be discussed later on, this setup of the bulge actually proved to be somewhat non-physical, however it did provide an interesting result.

### 3 Results

Before we move into the results of the paper, it is important to specify the values of the parameters presented in the previous section.

Parameter	Value	Units
$G$	$4.301 \times 10^{-6}$	$\text{kpc km}^2 \text{s}^{-2} M_{\odot}^{-1}$
$R_d$	2.0	kpc
$z_d$	0.15	kpc
$a_b$	0.25	kpc
$a_h$	5	kpc
$\alpha$	0.01	$\text{km}^2 \text{s}^{-2}$
$N_d$	100000	stars
$N_b$	18790	stars
$N_h$	10000	stars
$m_*$	1.0	$M_{\odot}$
$M_d$	100000	$M_{\odot}$
$M_b$	18790	$M_{\odot}$
$M_d$	10000	$M_{\odot}$

**Table (1)** Presented above are the values and corresponding units of each of the constants used in the equations introduced in the previous section. These constants were critical in initializing the galaxy.

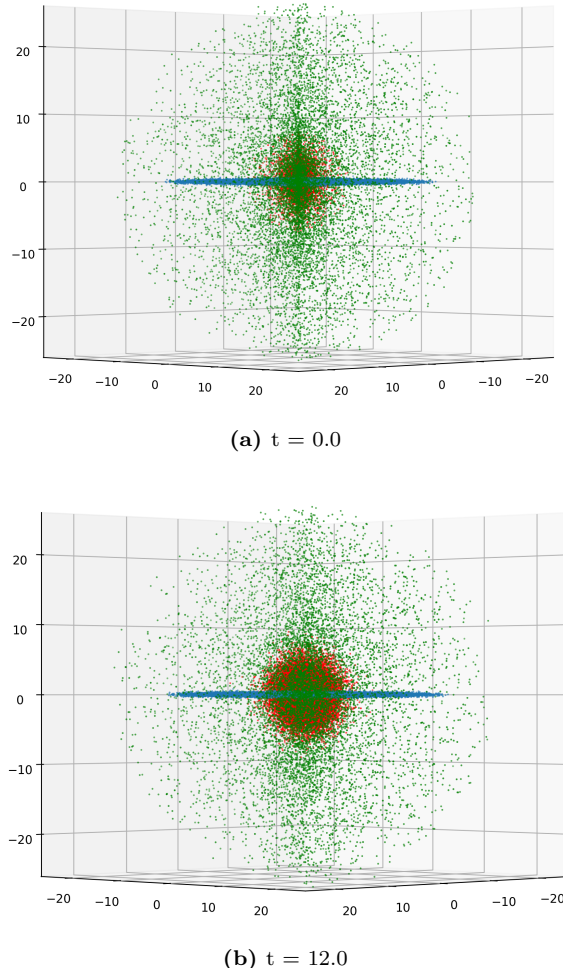
As can be seen in Table 1, the number of stars used to initialize the disk is exactly 10 times the amount used to create the halo, and about 5 times the amount used in the bulge. The bulge has an oddly specific number of stars due to a cutoff radius of  $30 a_b$  used in the simulation.

As mentioned in the introduction, there were three simulations run in total. The first contained all three of the stellar components: the disk, the halo, and the bulge. The second was run without the bulge. The third was run with an isolated disk.

It is important to note that for the first two simulations,  $t_{max} = 12.0$ , but for the third simulation  $t_{max} = 50.0$ , both given in terms of internal time units. The computational run-time for the first two was on the order of 5 hours, whereas for the isolated disk, it was less than one hour (even with a much larger maximum time). This is most likely due to the tree-selection algorithm in GADGET-2.

#### 3.1 The First Simulation

**Figure (1)** Below are the initial and final positions of the halo (green), disk (blue), and bulge (red). The coordinates of position are measured in kiloparsecs.



As mentioned before, this simulation involved all three of the stellar components of the galaxy: the disk, the halo, and the bulge. The following plots were of most importance in the

disk: surface density, vertical density, azimuthal velocity dispersion, radial velocity dispersion, and anisotropy. For the halo and the bulge, we look at the density profiles as well the radial velocity dispersion profiles. Also, as discussed before, the positions of stars and the rotational velocity distributions of each structure will also be critical in our analysis of the simulation.

As seen in Figure 1, the most obvious change between the initial time and the final time is the outward motion of the bulge stars. At first glance, this is probably due to an issue with the velocities, as is the case with most issues in N-body simulations. Further analysis of the density and dispersion profiles will help illuminate the causes and effects of this change.

A look at the bulge density profile over time shows that this outward motion is accretion-like in nature (see Figure 2). As time increases in the simulation, bulge stars gradually stream away from the center of the galaxy.

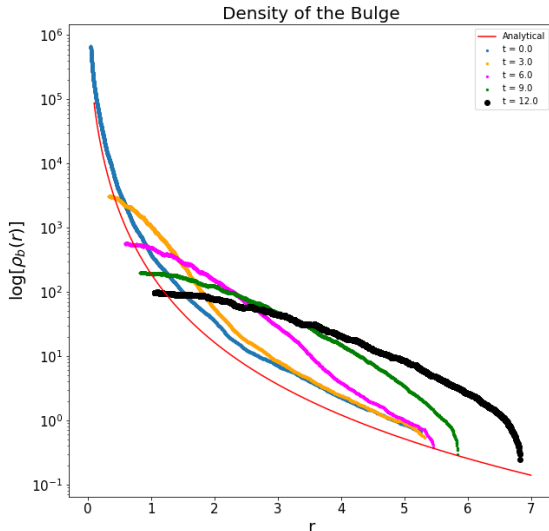


**Figure (2)** The density of the bulge as a function of radius, over different snapshot times. While the bulge starts close to the analytical profile, it shifts away as bulge stars move away from the center.

A look at the surface density of the disk also reveals a peculiar development. Figure 3 shows

that the surface density of the disk also has an apparent outward shift of stars, indicating that this phenomenon is not exclusive to the bulge. As will be discussed further in the next section, this could be an emergent property associated with the use of the spherical approximation in the disk, or it could be a normal effect in N-body simulations.

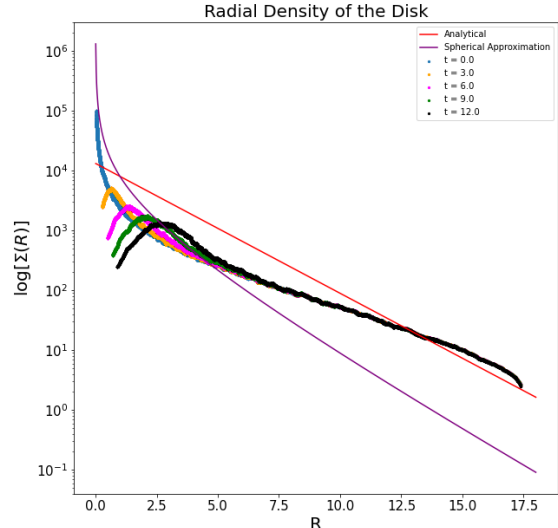


**Figure (3)** The radial/surface density of the disk as a function of the radius along the disk. Included is the analytical profile of the density (see equation 2), as well as the spherical approximation of the density.

The divergence of the surface density from the expected analytical profile is concerning at first. However, due to the complexity of initializing the disk and the further complexity of measuring the density in cylindrical shells, it is an acceptable result. For now, it will be appropriate to consider it somewhere in between the spherical approximation and the actual profile.

Since the radial (surface) density shows a long-term dynamical change, so does the vertical density ( $z$ -direction), as seen in Figure 4. Over time, the vertical density becomes “thinner”, suggesting that stars are tending towards the plane of the disk over time. This is not at all surprising due to the under-scaled  $z$ -direction velocity dispersion discussed in the previous section.

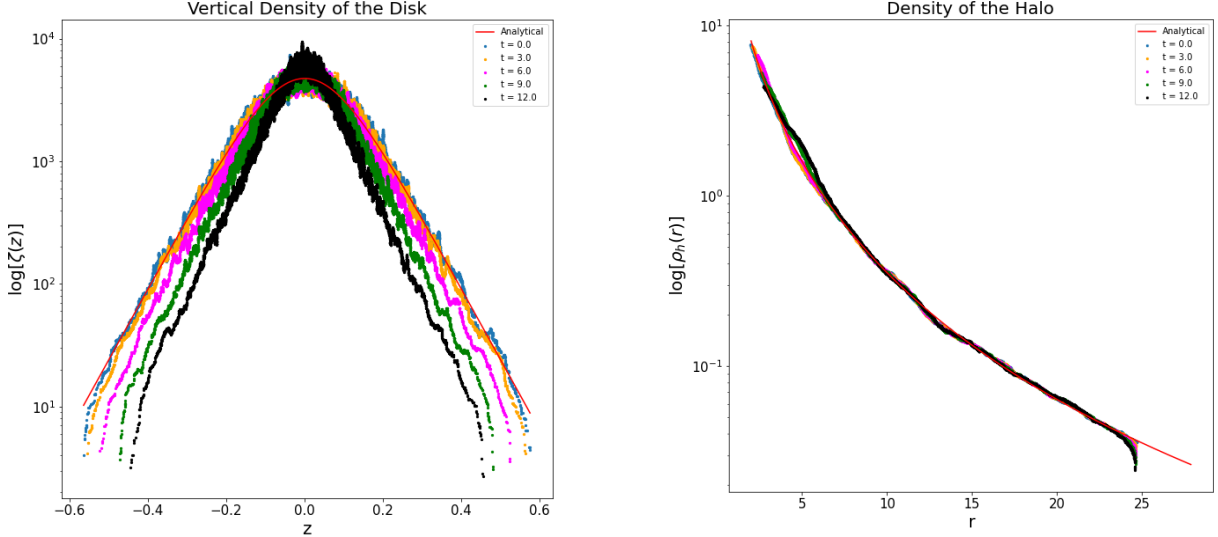


**Figure (4)** The vertical density of the disk as a function of  $z$ , distance from the plane of the galaxy. The analytical profile (see equation 2) is followed nicely for the first few snapshots, and diverges at outer  $z$  at later times.

One thing that has not yet been discussed is the way the dynamical effect seen in the bulge and disk has affected the halo. A quick glance at the halo density profile in Figure 5 shows that the halo is relatively unperturbed by the outward motion of bulge and disk stars. This is likely due to the distribution of the halo stars; their positions are too far away to be heavily affected by the dynamical effects in the bulge and disk.

Now that the density profiles have been scrutinized, our attention will shift to the velocity dispersion profiles. These will also demonstrate the dynamical effect seen in the positions and densities of the bulge and disk.

As seen in Figure 6, the radial velocity dispersion of the bulge diverges extremely from the analytical profile over time. By the final snapshot, the behavior of the profile has changed entirely from what it was initially.

Again, this outward shift of the bulge stars undoubtedly had an effect. It can be assumed that the outward shift caused there to be a change in

**Figure (5)** The density of the halo as a function of radius out from the center of the galaxy. As can be seen in the plot, there are very few halo stars within 4 kiloparsecs of center. The density varies little from the analytical profile over time.

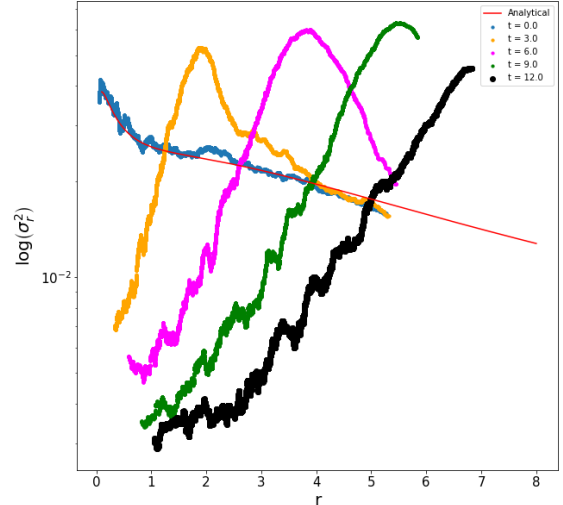


**Figure (6)** The radial velocity dispersion of the bulge as a function of time. While the initial snapshot agrees relatively well with the analytical profile, it does not take long for the profile to differ greatly.

the preferential direction in the radial velocity as time went on. The cause of this will be theorized in the next section.

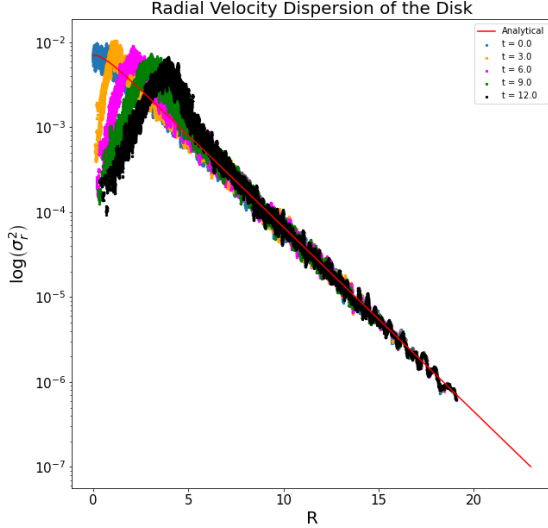


**Figure (7)** The radial velocity dispersion of the disk as a function of radius. Over time, a smaller but recognizable feature emerges in the inner part of the disk.

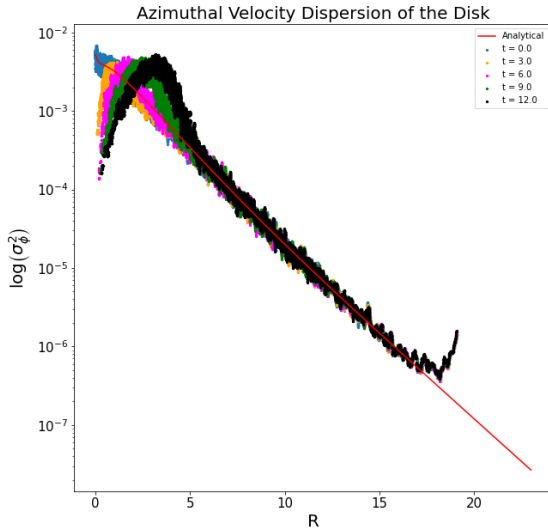


**Figure (8)** The azimuthal velocity dispersion of the disk as a function of radius. Again, over time, a similar feature emerges in the inner part of the disk.

While one might expect the radial and azimuthal velocity dispersions of the disk to also show drastic change over time, in correspondence with the bulge profile, this is not necessarily the case. As seen in Figure 7 and 8, there is a very slight change in both components of the velocity dispersion in the disk over the course of the simulation.

Specifically, this change occurs at a similar radius to the expansion of the bulge. This indicates that while the disk is apparently affecting the bulge stars, the reverse is also happening.

Again, it is possible that these phenomena could be caused by issues with the setup of the velocities, particularly in the bulge. But, it is important not to rule out a physical explanation.

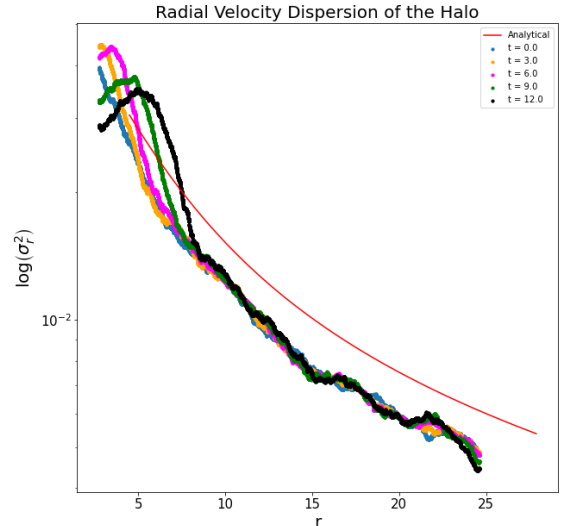


**Figure (9)** The radial velocity dispersion of the halo as a function of radius. Over time, a small shift occurs in the inner part of the halo.

Both components of the velocity dispersion of the disk mimic the profile formed by the bulge over time. There is the emergence of a “hump” of some sorts, with lower values of velocity dispersion at the inner side of the feature, and a return of the expected profile on the outer side. In fact, for both components, the analytical profile is followed closely in the mid-to-outer disk.

The radial velocity dispersion of the halo

provides some interesting information (see Figure 9). There is a slight deviation in the inner part of the halo from the analytical profile over time, suggesting that the motion of the disk and bulge stars may actually have had a greater effect than we initially realized.

We will finally turn our attention to the circular velocity profiles of each component at the beginning and end of the simulation. We will also look at the anisotropy of the disk over the course of the simulation. Anisotropy will be defined in the following manner:

$$\beta = 1 - \frac{\sigma_z^2 + \sigma_\phi^2}{\sigma_r^2} \quad (18)$$

Here, the equation strays slightly from the usual representation of anisotropy: it is in cylindrical coordinates instead of spherical. However, the use of  $\sigma_z^2$  assumes that the z-direction velocity dispersion is symmetric about the plane of the galaxy, which it is in analytical form.

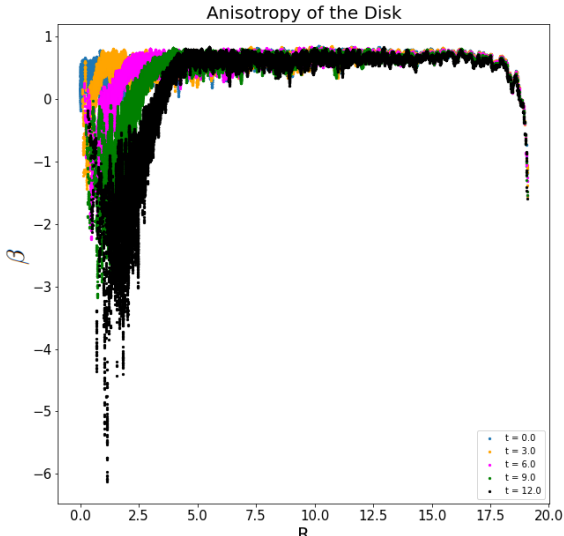
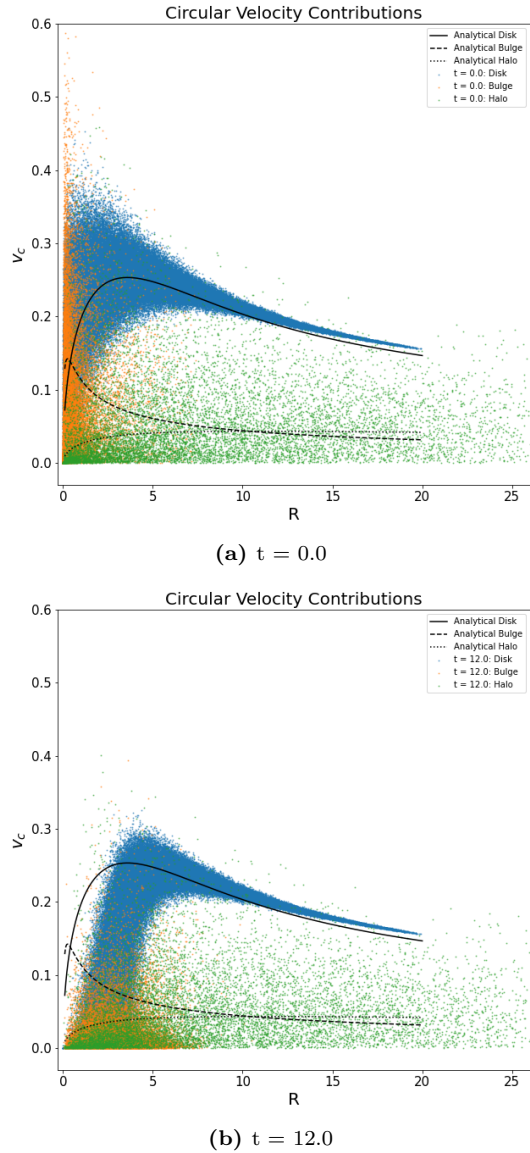


**Figure (10)** The anisotropy of the disk measured as a function of radius along the disk. There is a great deal of error in the measurement of the anisotropy, particularly as the time in the simulation progresses.

Figure 10 shows the anisotropy of the disk over the course of the simulation. As was expected,

there is again the emergence of a perturbing feature around the same place the feature appears in the density profiles and velocity dispersion profiles.

**Figure (11)** Below are the initial and final circular velocities of the halo (green), disk (blue), and bulge (red). The analytical profiles of each component are also included.



A look at the circular velocity plots at the beginning and end of the simulation also reveals a lot of information about the effect of that shift of stars in the bulge in the disk. Figure 11 clearly illustrates a shift inward of many disk and bulge stars, as well as a staunch decrease in the circular velocity of many inner disk and bulge stars.

As mentioned previously, the mid-to-outer disk is relatively unchanged, and while some halo stars are affected, the great majority of them also remain unperturbed.

This effect will be better illustrated in the isolated disk simulation, however the shift inward of the velocity profile is more than likely the result of the spherical approximation of the potential, or even could be an aspect of long-term simulations with an imperfect axisymmetric potential.

Nevertheless, the simulation including all three stellar components has illuminated many of the complexities of galactic dynamics. We will now shift our attention to the same simulation without the bulge.

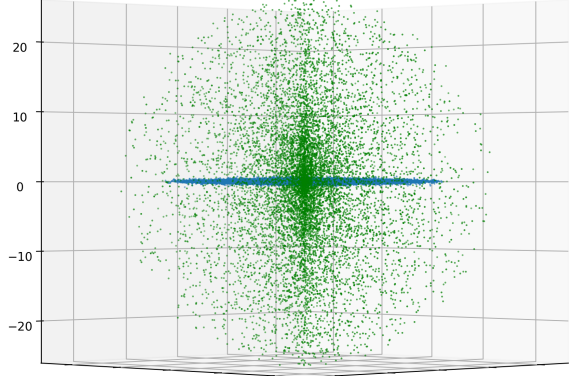
### 3.2 The Second Simulation

Now we will perform a similar set of analyses on the galaxy without the bulge. Our goal will be to see if the same dynamical effect occurs in the inner disk, and since there is no bulge, if it occurs it will be easy to determine that the motion of the bulge was *not* the cause, but an effect.

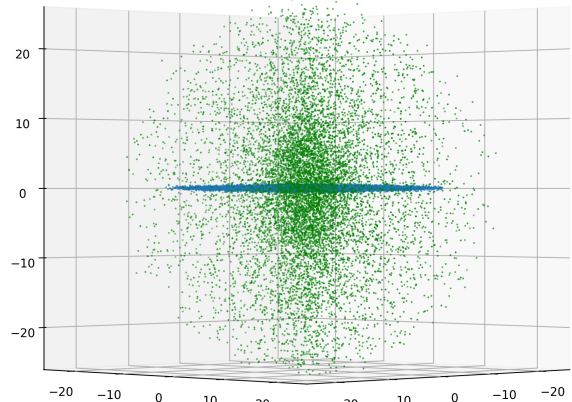
Like last time, we first look at the positions and how they change over time (see Figure 12). It is much less apparent than last time about any drastic change in positions over the course of the simulation. However, any change in the structure of the inner disk would not be easily seen in the figure.

Since there is no bulge to look at, it will be prudent to look at the surface density of the disk to see how it changed over the course of the entire simulation.

The most apparent thing about the density profile in Figure 13 is that while there is a “hump” feature emerging over time, just like the previous



(a)  $t = 0.0$



(b)  $t = 12.0$

**Figure (12)** Above are the initial and final positions of the halo (green) and disk (blue). The coordinates of position are measured in kiloparsecs.

simulation, it is less pronounced. It can be assumed that the existence of the bulge amplified the effect of this inward motion of disk stars.

Given that the surface density of the disk changed in a similar manner as the previous simulation, just less intensely, it would be expected for the vertical density to behave in a similar manner. As seen in Figure 14, the vertical density of

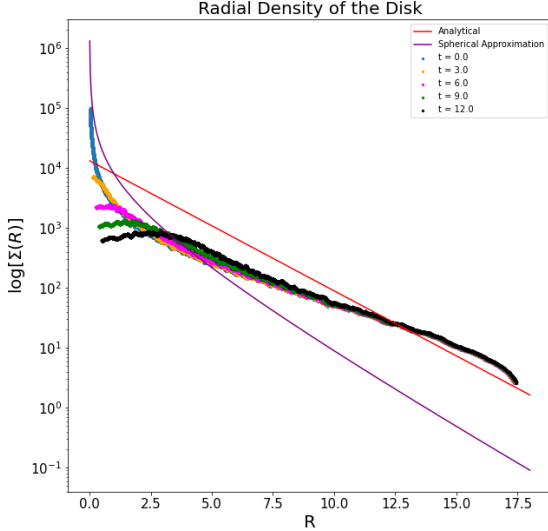


**Figure (13)** The radial/surface density of the disk as a function of the radius along the disk. Included is the analytical profile of the density (see equation 2), as well as the spherical approximation of the density.

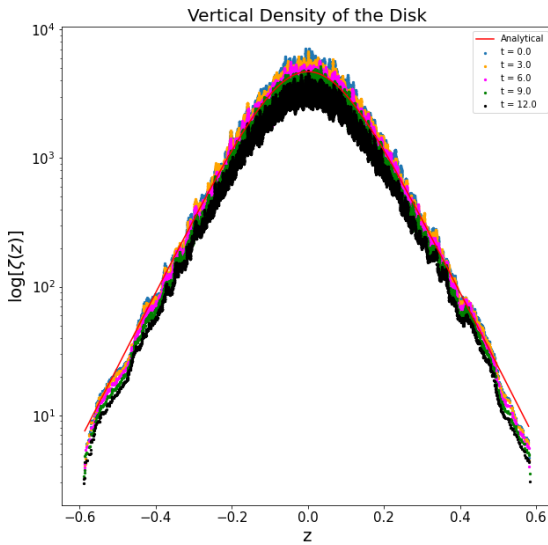


**Figure (14)** The vertical density of the disk as a function of the height above/below the disk. Included is the analytical profile of the density.

the disk gets thinner and thinner over time, as predicted. And again, as predicted, this effect is much less pronounced than it was with the inclusion of a bulge.

Given that the halo was relatively unperturbed even with the dynamical effect seen in the bulge and disk, it is expected that without the bulge, the halo will behave in a similar manner. Figure 15 shows the density of the halo, and, as just mentioned, there is very little that distinguishes this halo from the one in the previous simulation.

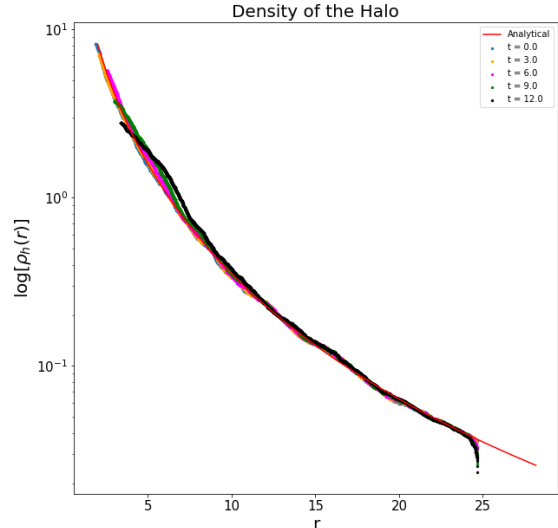


**Figure (15)** The density of the halo as a function of radius out from the center of the galaxy. The density varies little from the analytical profile over time.

After the density plots, the velocity dispersion plots will be important to look at. The radial and azimuthal velocity dispersion of the disk follows the same trend seen in the density profile when compared to the first simulation; the emergent effect is the same, but less pronounced. A comparison of Figures 16 and 17 with Figures 7 and 8 will support this claim.

The radial velocity dispersion of the halo, just like the dispersion profiles in the disk, matches the behavior of its predecessor, with less intensity. A quick glance at Figure 18 compared to Figure 9 will confirm this.

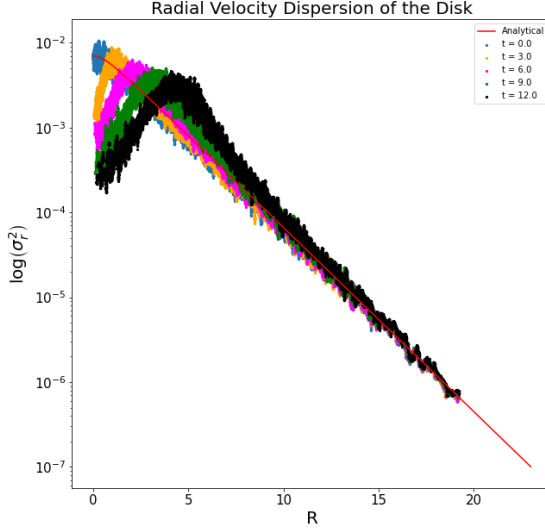


**Figure (16)** The radial velocity dispersion of the disk as a function of radius. Over time, a smaller but recognizable feature emerges in the inner part of the disk.

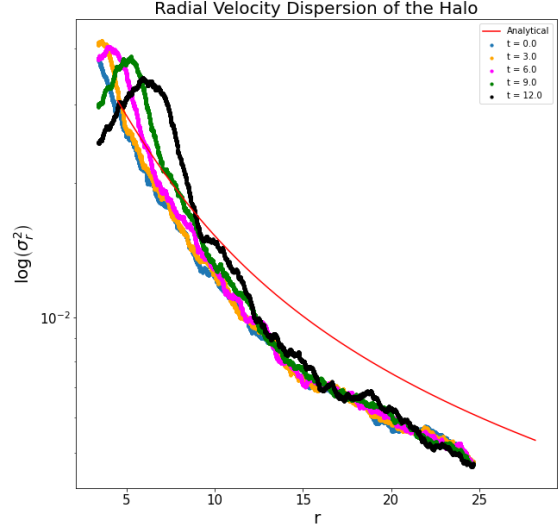


**Figure (18)** The radial velocity dispersion of the halo as a function of radius. Again, over time, a small shift occurs in the inner part of the halo.

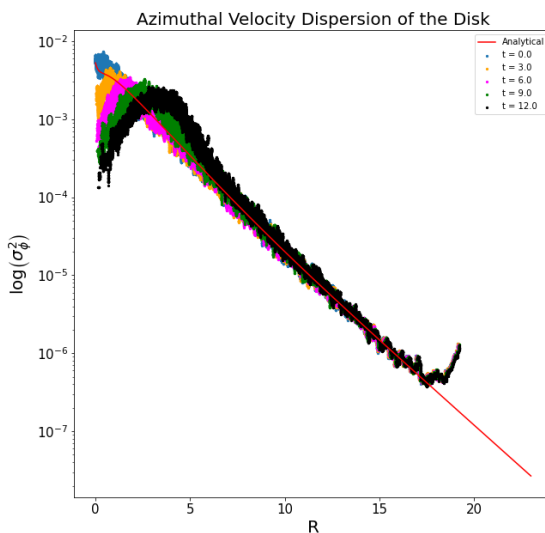


**Figure (17)** The azimuthal velocity dispersion of the disk as a function of radius. Again, over time, a similar feature emerges in the inner part of the disk.

What has been shown by looking at these dispersion plots is that while the bulge amplified the interaction seen in both the bulge and the disk in the previous simulation, the same effect occurs even without the bulge, with a lesser magnitude.

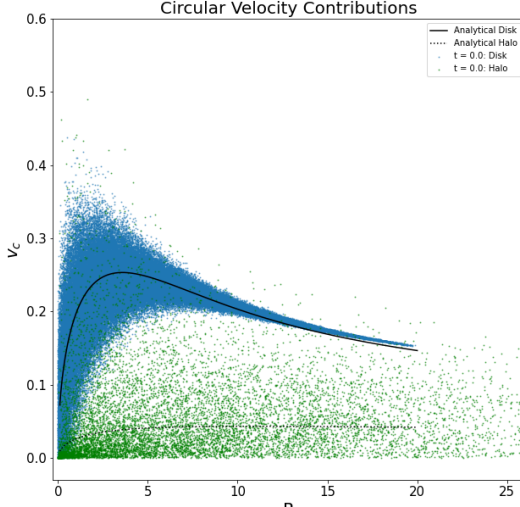
Therefore, it is safe to assume that whatever is causing this is located within the setup of the disk, or at the very least is an effect of the disk existing in the simulation.

Now, it is crucial to look at the development of the circular velocity of the disk and halo.

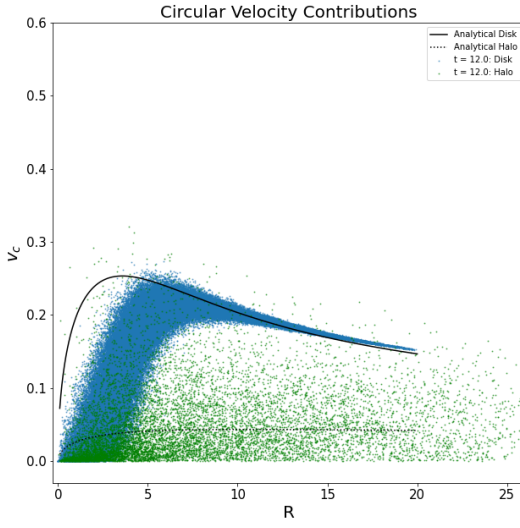
The anisotropy is not really worth looking at, as it illustrates the same trend seen with the velocity dispersion profiles of the disk; the profiles follow the same behavior as they did in the first simulation, but to a lesser extent.

The circular velocity also reflects this dynamic by showing that inner disk stars are again losing circular velocity and shifting outward in radius (see Figure 19).

An analysis of the radial velocity would demonstrate the opposite effect: the inner disk stars would gain radial velocity over the course of the simulation.



(a)  $t = 0.0$



(b)  $t = 12.0$

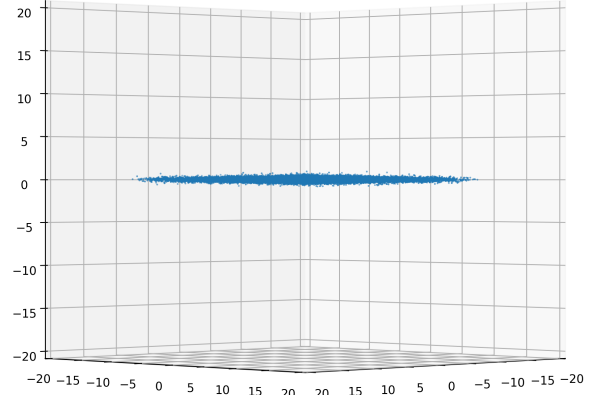
**Figure (19)** Above are the initial and final circular velocities of the halo (green) and the disk (blue). The analytical profiles of each component are also included.

### 3.3 The Third Simulation

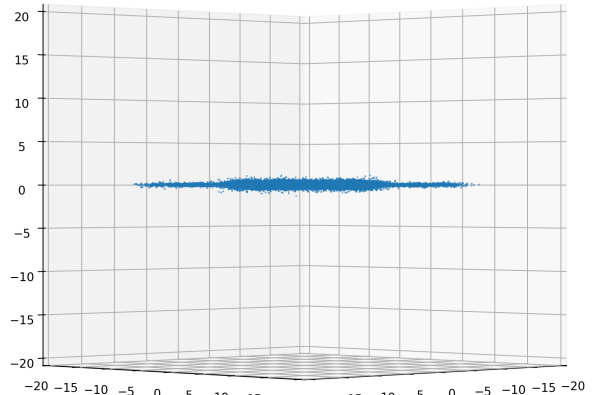
The third and last simulation was run with just the disk, which was setup in the same manner as the previous two simulations.

A key difference between the other two simulations and this one is that due to the much faster run-time of GADGET-2 with just a disk, a maximum time of  $t_{max} = 50.0$  was used as opposed to the value of 12.0 used in the other two.

**Figure (20)** Below are the initial and final positions of the disk (blue). The coordinates of position are measured in kiloparsecs.



(a)  $t = 0.0$



(b)  $t = 50.0$

The outward movement of the inner disk is the most apparent feature when looking at the comparison of the positions of the disk stars at the beginning and end of the simulation. As will be seen shortly, due to the longer run-time, the disk had more time to dynamically evolve, and the results are extremely interesting.

In Figure 21, we see the evolution of the radial density of the disk. Now it is obvious what the dynamical interaction seen in the previous two simulations was leading to. The “hump” feature becomes more and more defined throughout the course of the simulation. As will be discussed in the next section, it is entirely possible that the radial velocity noise assigned to the disk is causing this shift in the inner disk stars.

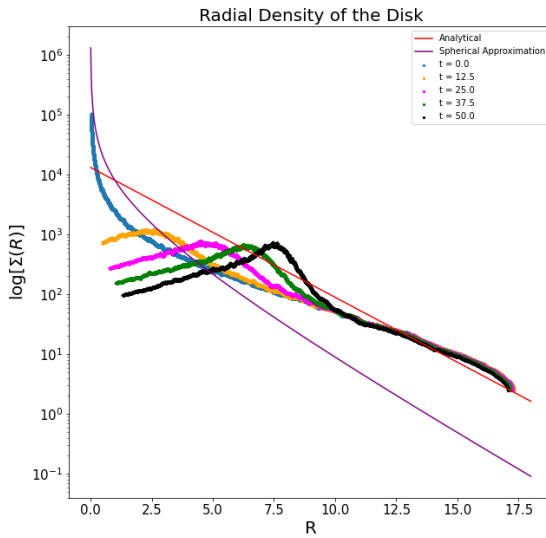


**Figure (21)** The radial/surface density of the disk as a function of the radius along the disk. Included is the analytical profile of the density, as well as the spherical approximation of the density.

A look at the vertical density of the disk confirms what was expected (see Figure 22); a more drastic “thinning” motion of the density profile over the course of the simulation. As mentioned before, this migration of disk stars towards the plane of the disk suggests that the velocity dispersion in the z-direction was under-scaled.

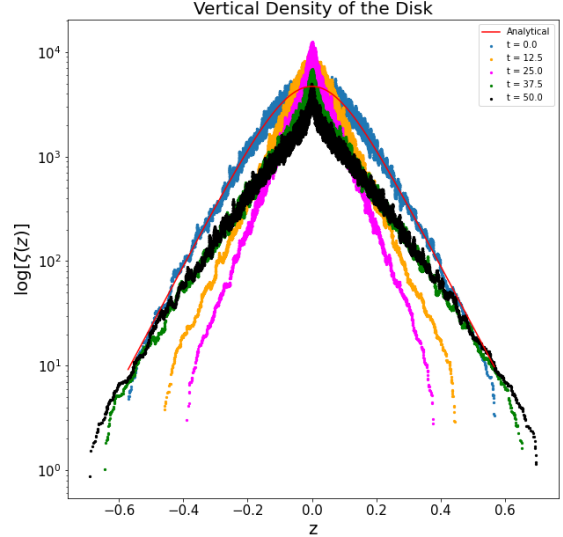


**Figure (22)** The vertical density of the disk as a function of the height above/below the disk. Included is the analytical profile of the density.

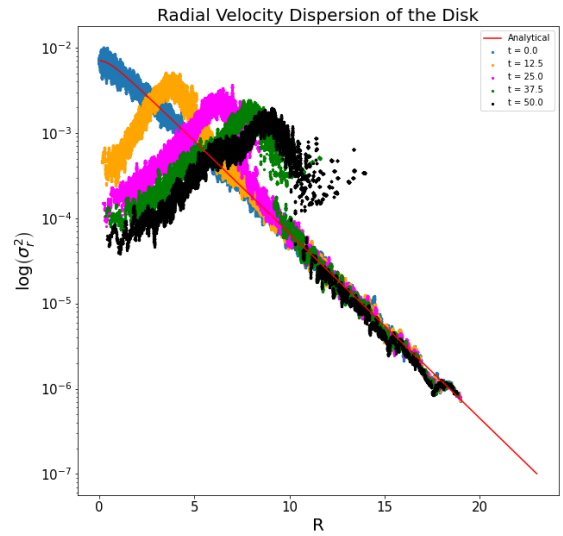


**Figure (23)** The radial velocity dispersion of the disk as a function of radius. Over time, a break in the profile emerges in the inner-to-middle part of the disk.

The velocity dispersion profiles are also interesting. In both the radial and azimuthal directions (Figures 23 and 24, respectively), as the “torus-like” feature in the inner-mid disk forms, there is a larger and larger break formed in the velocity dispersion profiles.

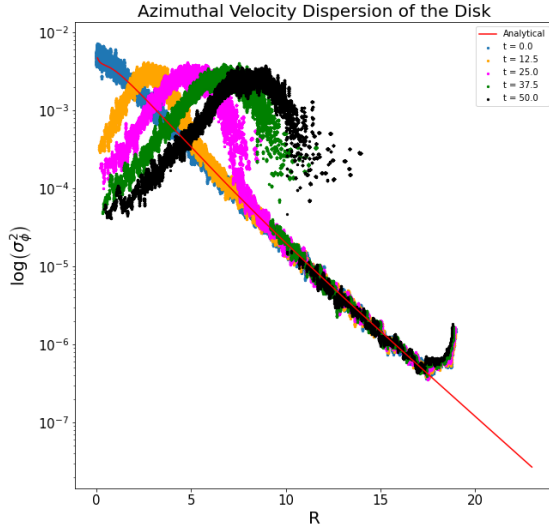


**Figure (24)** The azimuthal velocity dispersion of the disk as a function of radius. Again, over time, a break in the profile emerges in the inner-to-middle part of the disk.

The break in these profiles is an effect of how the dispersion is measured (binning shells of stars and then taking the standard deviation), but also suggests a rapidly changing dispersion as a function of radius at the break.

A look at the anisotropy of the disk shows the effect of these breaks as well (see Figure 25). Clearly, whatever feature is forming in the disk (the “torus”) is having a drastic effect on the stars in the surrounding regions of the disk.

While there is not as apparent of a break in the anisotropy profile, there is clearly an all-too-familiar “hump” formed in the profile, the peak of which gradually shifts outward.

In retrospect, reducing the noise associated with the anisotropy and dispersion profiles would have been an effective measure when setting up the

simulation and analyzing the snapshots.

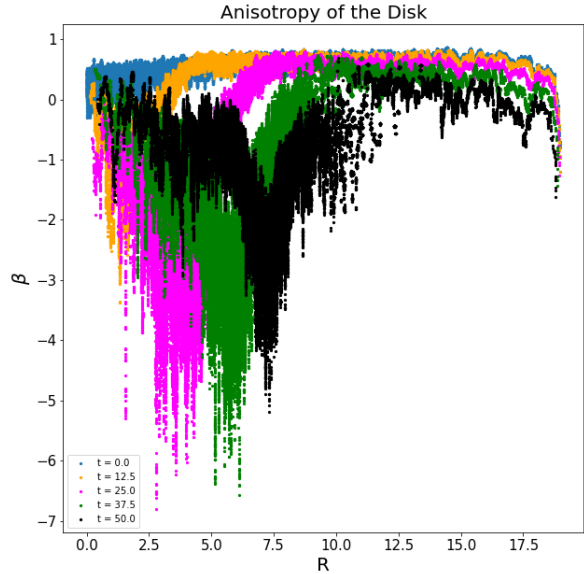


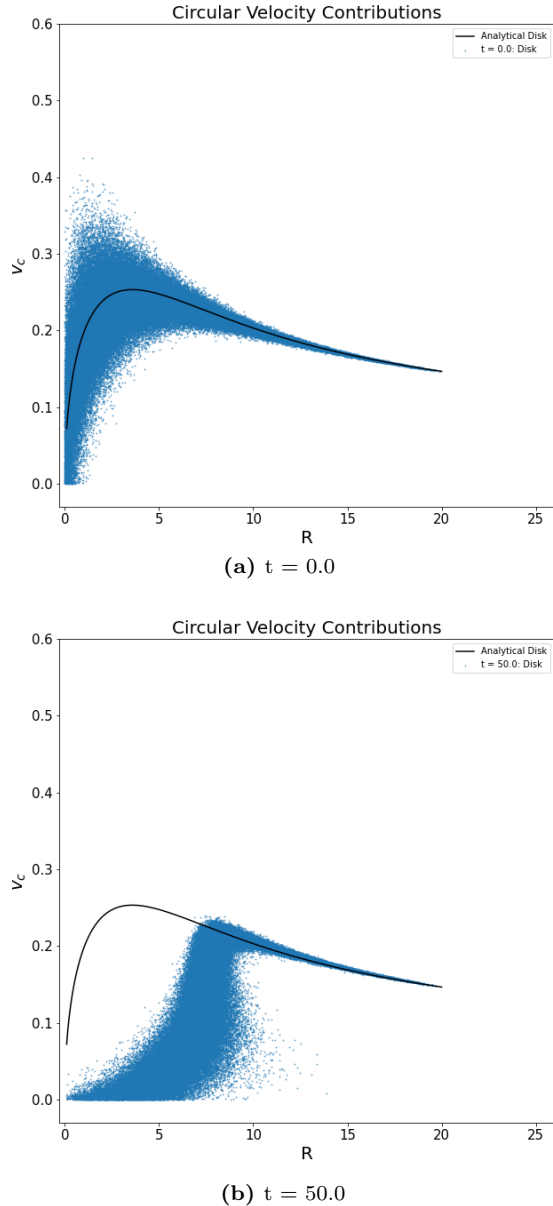
**Figure (25)** The anisotropy of the disk measured as a function of radius along the disk. There is a great deal of error in the measurement of the anisotropy, particularly as the time in the simulation progresses.

The circular velocity profiles also shed some light on this emergent feature in the disk. Figure 26 shows that by the end of the simulation, a great deal of disk stars have moved outward, as if following a type of wave.

Interestingly, the outer disk is once again relatively unperturbed. I would have expected this feature to have at least lightly distorted the outer rotation curve of the disk, but there is only a very minimal shift of the mid-to-outer circular velocities over the course of the simulation.

Now that the results of all three galactic simulations have been presented, it is time to discuss the implications. It will also be productive to discuss some potential fixes for future simulations, from the initialization of the stellar components to computational methodologies.

**Figure (26)** Below are the initial and final circular velocities of the disk. The analytical profile of the disk is also included. It is clear that the movement of inner disk stars outward into the emergent “torus” feature severely distorted the inner rotation curve.



## 4 Discussion

The main takeaway from the results of all three of the simulations is the time-dependent development of this peculiar feature in the inner disk, which also has an effect on the bulge when it is included in the simulation.

As discussed before, the most likely explanation for the growth of the bulge is an error in the initialization of the velocities. The assumptions made about isotropy and the radial velocity dispersion of the bulge diverged from the methodologies of Hernquist and other N-body simulations, so fixing the velocities in the bulge might stop the outward motion of the bulge stars over time.

However, given that the disk stars showed a similar behavior, regardless of the inclusion of a bulge or not, this may suggest that fixing the bulge velocities alone would not stop the outward growth of the bulge.

In fact, the main culprit behind the emergence of this feature in the disk and bulge might actually be the radial velocity dispersion of the disk. If there was a scaling error (i.e. over-scaled) in the initialization of the disk, this would have caused the radial velocities (which were chosen from noise generated by the dispersion) to have been scaled too high in the inner regions of the disk. This, in turn, would lead to many inner disk stars moving outward over the course of the simulation, which is what we see.

Another issue with the disk was the z-velocity dispersion, which as mentioned many times previously, was severely under-scaled due to the use of an undervalued  $\Sigma(0)$ . This value, which represents the central surface density of the disk, was taken to be 1, when it is actually much higher (by a factor of about 1000).

The halo, in comparison to the disk and bulge, behaved in a much more physical way. This was confirmed by the density and velocity dispersion profiles and the manner in which they closely followed the analytical profile throughout the simulation.

In retrospect, setting up a dark matter halo with mass substantially greater than the disk would

have been interesting, especially in terms of its effect on the disk and bulge. Would the disk feature have formed as dramatically with a dark matter halo instead of just a luminous halo?

In fact, in order to estimate the order of magnitude of the dark matter halo mass, we can look at the analytical rotation curves and determine a dark matter halo that flattens the rotation curve in the outer regions of the galaxy. It is assumed that the dark matter halo follows the NFW density profile (see equation 11).

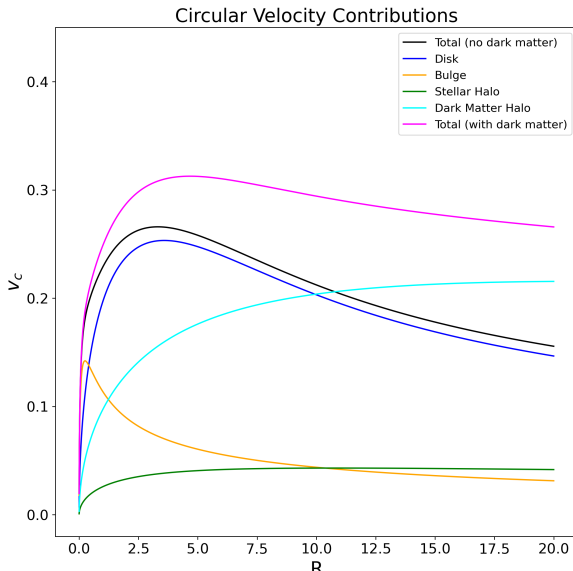


**Figure (27)** This figure shows the rotation curve of the disk (blue), stellar halo (green), bulge (orange), total with no dark matter (black), dark matter halo (cyan), and the total with all components included (pink).

The dark matter halo used in Figure 27 had the following parameters:  $a_{dm} = 10$  and  $M_{dm} = 5M_d$ . Clearly, if a simulation including this dark matter halo were to be run, one would either have to allocate more computational power, run-time, or reduce the mass of the disk (i.e. reduce the number of stars in the disk), so as to scale down the number of dark matter particles.

Alternatively, the mass of each dark matter halo particle could be scaled up, but this might lead

to some gravitational issues in the inner regions.

Moving back to the disk, it is possible that even with enacting all of the changes to the velocities of the inner disk and bulge, as well as adding a dark matter halo, that the feature in the disk could still emerge. This could be due to a failing with the spherical approximation of the disk potential, but also could be due to something inherent in axisymmetric disks with noise.

The McMillan paper discusses the emergence of bars and spiral arms in the evolution of axisymmetric disks. Although we do not see that in our simulation, it is possible that the development of this "torus" feature is actually the spherical equivalent. It may be that the way the disk was initialized on the spherical approximation of the exponential disk profile restricted the emergence of non-axisymmetric modes such as a bar or arms.

As was noted previously, there was also an issue in matching the density profile of the disk to the analytical profile. Whether or not this was an issue with how the density profile was measured (i.e. the cylindrical shell method) or this was a mathematical issue in assigning the positions of the disk stars is unclear. However, if this issue was also fixed (if it is a positional issue), it may also allow for the emergence of these anti-axisymmetric phenomena, or at the very least fix the issue of the "torus" forming.

It would be prudent for future simulations to make the necessary changes mentioned here, and then to see if the feature in the disk still emerges. If it does, it might point towards the feature being the spherically symmetric version of a bar or arm. If not, then it likely has no physical meaning, and was purely an error computationally in the setup of the disk.

Ideally, the results presented in this paper have demonstrated the complexity behind N-body simulations, as well as the inherent beauty hidden in our limited understanding of galactic dynamics.

## 5 Appendix

It should be noted that for the purposes of some of the equations (i.e. escape velocity, etc.), as well as some of the background information, the classic text [Binney & Tremaine \[1\]](#) was used.

To access the files used in the creation of the simulations and the plots, visit [this link](#). Also, it should be noted that some of the scripts utilized in the repository were adapted and changed for each simulation (i.e. the bulge was removed, then the halo, etc.).

## References

- [1] James Binney and Scott Tremaine. *Galactic dynamics*. 2nd ed. Princeton series in astrophysics. Princeton: Princeton University Press, 2008. ISBN: 9780691130262 9780691130279.
- [2] Lars Hernquist. “An analytical model for spherical galaxies and bulges”. In: *The Astrophysical Journal* 356 (June 1990), pp. 359–364. ISSN: 0004-637X. DOI: [10.1086/168845](https://doi.org/10.1086/168845). URL: <http://adsabs.harvard.edu/abs/1990ApJ...356..359H> (visited on 04/25/2021).
- [3] Lars Hernquist. “N-Body Realizations of Compound Galaxies”. en. In: *The Astrophysical Journal Supplement Series* 86 (June 1993), p. 389. ISSN: 0067-0049. DOI: [10.1086/191784](https://doi.org/10.1086/191784). URL: <https://ui.adsabs.harvard.edu/abs/1993ApJS...86..389H/abstract> (visited on 04/25/2021).
- [4] Paul J. McMillan and Walter Dehnen. “Initial conditions for disc galaxies”. In: *Monthly Notices of the Royal Astronomical Society* 378.2 (June 2007). arXiv: astro-ph/0703534, pp. 541–550. ISSN: 0035-8711, 1365-2966. DOI: [10.1111/j.1365-2966.2007.11753.x](https://doi.org/10.1111/j.1365-2966.2007.11753.x). URL: <http://arxiv.org/abs/astro-ph/0703534> (visited on 04/25/2021).
- [5] Julio F. Navarro, Carlos S. Frenk, and Simon D. M. White. “The Structure of Cold Dark Matter Halos”. In: *The Astrophysical Journal* 462 (May 1996), p. 563. ISSN: 0004-637X. DOI: [10.1086/177173](https://doi.org/10.1086/177173). URL: <http://adsabs.harvard.edu/abs/1996ApJ...462..563N> (visited on 04/25/2021).
- [6] Volker Springel. “The cosmological simulation code GADGET-2”. In: *Monthly Notices of the Royal Astronomical Society* 364.4 (Dec. 2005). arXiv: astro-ph/0505010, pp. 1105–1134. ISSN: 0035-8711, 1365-2966. DOI: [10.1111/j.1365-2966.2005.09655.x](https://doi.org/10.1111/j.1365-2966.2005.09655.x). URL: <http://arxiv.org/abs/astro-ph/0505010> (visited on 04/25/2021).